Presented at the 33rd IEEE Photovoltaic Specialists Conference, San Diego, CA 13 May 2008
Area 2, paper #709

MEASURING CdS/CdTe BACK CONTACT BARRIER HEIGHTS BY INTERNAL PHOTOEMISSION

Alan Fahrenbruch <alanf@stanford.edu>
Department of Physics, Colorado State University
Fort Collins, CO 80523

ABSTRACT

The back contact of the CdS/CdTe solar cell is one of the most critical aspects in optimizing efficiency and stability. A fundamental parameter is the barrier height Φ_{bc} and its measurement is important to fully understanding the device.

Plotting the Internal photoemission (IPE) current response to sub-band-gap light according to the Fowler theory gives an intercept equal to the barrier height. IPE can be applied to completed cells, and to thick, thin, and n/i/p cells. Results are compared for a number of cells from various fabricators, including those with good and bad contacts and electronically thick and thin cells. Results suggest two barriers in parallel: a high one, (~ 0.9 eV) which agrees well with the observed UPS values and a low one (~ 0.3 eV) with a much smaller area fraction (1 - 4%) which dominates the contact transport and corresponds more closely to the values observed for efficient cells. For thick cells, IPE results agree well with thermal measurements.

PERSPECTIVE

The back contact may be the least understood part of the CdS/CdTe solar cell—but one of the most crucial. The back-contact barrier height Φ_{bc} is a fundamental parameter and its measurement is important to understanding and optimizing these devices. Optimization of the back contact is hampered by lack of direct feedback, especially due to its strong interaction with other the parts of the cell and the necessity of measuring it in the cell after processing.

For single-crystal (SX) CdTe, the barrier height to a metal contact Φ_c is partially pinned by interface dipoles and only reluctantly follows the difference between the electron affinity of the CdTe χ and the work function of the metal ϕ_m. SX measurements range from Φ_c = 0.85 to 1.18 eV for metal work functions from 5.6 to 4.2 eV. [1]. Späth et al. [2] find Φ_c = 0.7 - 0.8 eV for polycrystalline (PX) CdTe/Cu_xTe contacts by UPS measurements. However, for CdTe-based cells to be as efficient as they are, the back contact barrier height Φ_{bc} must be less than ~ 0.4 eV (call this the cell limit) and so the observed SX and PX values are much too high. This conceptual problem is usually resolved by invoking tunneling through the CdTe adjacent to the contact [1,2].

For the case of electronically thick cells, the depletion layers of the main CdS/CdTe junction and the back contact junction are spatially separated and don't interact. For these devices, Φ_{bc} can be determined accurately by measuring the activation energy of the high forward-bias current above V_{oc}, in the dark or light. Values of Φ_{bc} in the 0.3 to 0.6 eV range are obtained [3-6]. Few systematic Φ_{bc} measurements vs. cell properties or fabrication variables have been reported in the public literature.

However, for electronically thin and n-i-p cells, where the high forward-bias current often depends strongly on bulk transport (e.g., in the p-CdTe), thermal methods can be ambiguous. Since the built-in voltage of n/i/p devices and hence their efficiency is determined by $E_g - \Phi_{bc}$, where E_g is the band gap, it is important to measure Φ_{bc} accurately in order to understand and improve these cells. [7]

Another method of determination of Φ_{bc}, Internal Photoemission (IPE) is explored here and compared with thermal methods for several different types of CdS/CdTe cells, including devices with good and bad contacts, and thick and thin cells.

INTERNAL PHOTOEMISSION BACKGROUND

In the simplest form of Internal Photoemission (IPE), the contact is illuminated with sub-CdTe-band-gap light through the front window of the device. Holes with energies greater than Φ_{bc} are able to scatter into the semiconductor and be collected by the barrier field (Fig. 1) and the hole current I_{pe} is measured as a function of photon energy $h\nu$. The quantum efficiency $QE_{pe} = I_{pe}/q\Gamma$, where Γ is the incident photon flux, plotted as $(QE)^{1/m}$ vs. $h\nu$ (where m = 2 to 3), yields an intercept equal to the barrier height (Fig. 2). IPE has been used extensively for many years to measure semiconductor/metal contact barrier heights [8].

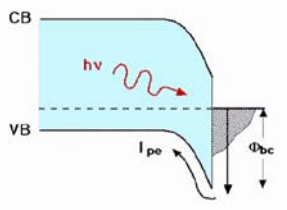

Fig. 1. Contact band diagram.

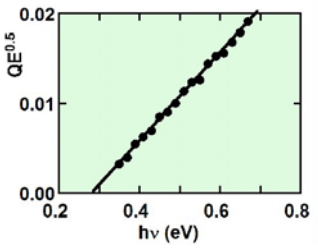

Fig. 2. Fowler plot.

The original theory, put forth by Fowler [9] for emission from metals into a vacuum, has been extended to semiconductors. For $h\nu > \Phi_c + 3$ kT, it can be approximated by:

$$QE_{pe} = C_f (h\nu - q\Phi_c)^m \quad ...(1)$$

where m = 2 for the Fowler theory and C_f is nearly constant. In this paper, the original, unapproximated form which expresses the temperature dependence is used.

URBACH TAIL ABSORPTION

The Urbach optical absorption tail extends exponentially below the band gap [10] and the current resulting from this absorption is in the same direction as the conventional J_{sc}. The quantum efficiency QE for a cell, shown in Fig. 3, includes both the Urbach tail and the response above the band gap. This data shows an Urbach energy E_{Ur} ~ 35 meV at 1.3 eV. The Urbach energy is a measure of disorder and this value can be compared to 7.6 meV for chemically polished single-crystal CdTe by Marple [11] and 28 meV for polycrystalline CdTe thin films by Fischer et al. [12].

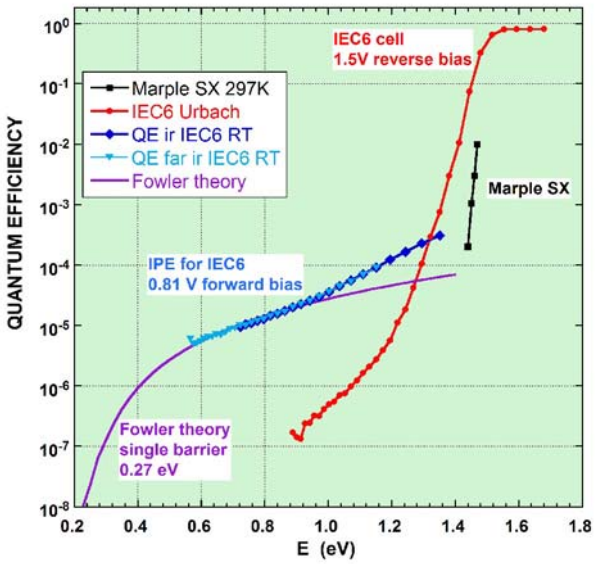

Fig.3. Quantum efficiency data for:
(a) CdS/CdTe cell at 1.5 V reverse bias,
(b) from absorption data, Marple, X 1e-4, for SX CdTe,
(c) IPE yield for an IEC cell at 0.81 V forward bias, and
(d) a theoretical Fowler curve for single 0.27 eV barrier.

Also shown in Fig. 3 is a representative IPE QE, taken at a forward bias of ~ 0.81 V for the same IEC cell, opposite in sign to J_{sc}. A Fowler theory curve for a single 0.27 eV barrier is shown as well. For large E_{Ur}, the IPE data may be affected by the Urbach current at higher photon energies.

BIAS VOLTAGE

At zero or reverse bias the sensitivity to the already small IPE currents generated at the back contact is strongly diminished by the impedance of the main junction. The signal can be dramatically increased by running the cell at forward bias to decrease the dynamic resistance of the main junction. The contact is excited with chopped light and the ac voltage developed by the IPE current through a measuring resistor R_m is picked off by a capacitor and directed to a lock-in amplifier (LIA). Operation at forward bias also suppresses the Urbach current, and increases the collection field for holes. However it raises the possibility of secondary photoconductivity.

SECONDARY PHOTOCONDUCTIVITY?

There is some uncertainty as to whether the observed "IPE" current arises from internal photoemission or from Secondary Photoconductivity (SPC). SPC has been observed in n/p/n junctions [13] and a-Si:H devices [14,15] in forward bias, when carriers can be replenished at the contacts. On exposure to light, this could arise from either (1) an increase in the minority carrier density in the p-CdTe or (2) a change in the charge density in the p-CdTe by filling or emptying mid-gap states which lowers the bands (similar to a phototransistor effect).

I believe that the minority carrier density increase can be ruled out because it should be fully included in the "Urbach" current, measured at reverse bias, which was found to be much smaller than the IPE current at low photon energies (< 1.2 eV) (Fig. 3). For energies above ~ 1.2 eV, it might have some effect, however.

Considerations about the modulation of the bands of the main junction include:

1. A small (< ~1%) modulation of dark forward-bias current after application of strong (I_{sc} ~ 12 mA/cm^2) 780 nm light pulses is observed in some of these cells for V ~ V_{oc}. However, the time constant for decay of this transient is several seconds whereas the IPE signal, usually measured at a chopper frequency of 327 Hz, is relatively insensitive to frequency over the range 100 Hz to 770 Hz at RT. In addition this modulation decreases rapidly as photon energy and/or intensity is decreased.
2. The IPE signal increases as forward bias increases, closely following the results of a lumped-parameter equivalent circuit model (which does not include SPC). In most cases, the IPE signals were obtained at biases between V_{oc} and the cross-over point, where illumination affects the junction current only weakly. The shapes of the low energy part of the IPE curves are insensitive to bias voltage.
3. The IPE signal increases strongly as T decreases, as predicted by the lumped-parameter equivalent circuit model. This is because the dynamic impedance of the contact barrier increases, while that of the main barrier is kept small by forward bias.
4. The low barrier parts of the IPE curves do fit the Fowler plot formalism with QE = $C(h\nu - \Phi_{bc})^m$ and m = 2, with absolute quantum efficiencies close to the expected values.
5. The Fowler thresholds obtained are in good agreement with the Φ_{bc} values obtained from drift/diffusion thermal measurements.

Given these considerations, I think that the current due to internal photoemission from the contact is considerably larger than that from SPC at low photon energies, but I can't definitively rule out the possibility of an SPC effect at this time.

EXPERIMENTAL CONSIDERATIONS

A 250 W quartz-halogen lamp, powered by a current-controlled dc power supply was used. This was followed by a chopper, a PTI 0.25 m monochromator, blazed at 1000

nm, a mechanical shutter and order-sorting filters: Corning 2-64 glass for 1.4 < hν < 1.7 eV, 0.5 mm thick SX GaAs for 0.78 < hν < 1.38 eV, and 3 mm thick SX Si for 0.6 < hν < 1.03 eV. The current-equivalent photon flux at the cell was on the order of 10 mA/cm^2 at 1 eV. All IPE data were taken with SX filters. The samples were mounted in a vacuum cryostat, with a LakeShore 330 controller. The cells were driven by batteries to reduce noise, and the signal was output to an SRS 510 lock-in amplifier. SPICE modeling was invaluable in choosing the circuit values of the measuring resistance and coupling capacitor. The QE results shown are absolute to within ± 20%, rather than being relative or arbitrary units (except for IEC6 on Fig. 4).

INTERNAL PHOTOEMISSION RESULTS

Measurements were done on three groups of cells: (a) electronically thick cells (IEC, CdTe ~ 7 μm), (b) thin cells (CdTe ~ 1.8 μm), and (c) thick cells (NREL) with ZnTe back contacts. We start with a "normal" IEC cell and then detail and compare the other cells in later sections.

IEC Thick Cells

Data for "IEC6 with Cu" (a normal, electronically thick cell with a good contact), plotted as QE$^{0.5}$ vs hν in Fig. 4, shows two branches.

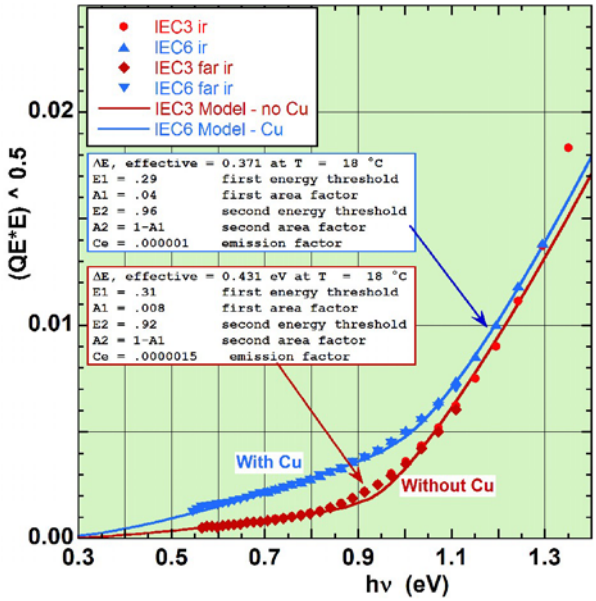

Fig.4. (QE)$^{0.5}$ vs. hν for IEC6 cell (with Cu) and IEC3 (without Cu) at 18°C. Points are measured data and curves are for model. The QE for IEC3 is absolute, but the QE for IEC6 has been multiplied by 12.5.

This shape was common to most of the cells and suggests a composite of two barrier heights. The IPE QE was modeled as the sum of contributions from barriers of two different heights Φ_1 and Φ_2 [as was done by 16] using the full, un-approximated Fowler expression. The emission coefficient (e.g., the prefactor in Eq. 1) for the metal for both the barriers is assumed here to be the same. Each of the barriers have separate collection coefficients, C_1 and C_2. Among the possible physical models for the collection coefficients are:

1. The composite barrier consists of two barriers in parallel, so that the collection coefficients are proportional to the area of each barrier, $C_1 = C_{c1}A_1$ for the low barrier at Φ_1, with $A_2 = 1–A_1$, so $C_2 = C_{c2}(1–A_1)$. The C_{c1} and C_{c2} factors might, for example, depend on the electric field at the interface.
2. The composite barrier includes transport over a barrier of height Φ_2 and tunneling through the same barrier at an average energy Φ_1. Then $C_1 = T_rC_{c1}$., where T_r is the effective tunneling transmission probability at Φ_1 and $C_2 \sim C_{c2}$.

It is not obvious how the IPE experiment could distinguish between these options; IPE gives us only the two threshold energies and the ratio between C_1 and C_2. We proceed by assuming option 1, the areas in parallel, and that $C_{c1} = C_{c2}$. For the model, the QE for each barrier, weighted by C_1 and C_2, were summed and plotted as QE$^{1/2}$. The model showed good agreement with the data. An effective barrier height $\Phi_{bc,eff}$, as if the same current were going over a single barrier, could then be calculated assuming thermionic transport using:

$$\Phi_{bc,eff} = - kT \log[A1 \exp(-\Phi_1/kT) + (1-A1) \exp(-\Phi_2/kT)]. \quad \ldots(2)$$

Using a drift/diffusion model here makes only small changes in $\Phi_{bc,eff}$.

For IEC6, with a Cu-diffused back contact, the low barrier Φ_1 = 0.29 eV and Φ_2 = 0.96 eV, giving an effective barrier $\Phi_{bc,eff} \sim 0.37$ eV. In this model the low barrier area is ~ 4% of the total area.

Similar measurements on a cell with a bad back contact with severe roll-over, IEC3 (without Cu), indicate a significantly larger $\Phi_{bc,eff} \sim 0.44$ eV (Fig. 4) with Φ_1 = 0.31 eV and Φ_2 = 0.94 eV, but a significantly smaller A_1 = 0.7%.

If one proceeds with the parallel barrier area hypothesis then the change in barrier height is due to a reduction in the low contact barrier area by a factor of 6. This is illustrated in Fig. 4, where the IEC3 and IEC6 QE curves are adjusted to match in the 1.1 - 1.3 eV range before both are plotted as QE$^{0.5}$. In this plot the high barrier height intercept at ~ 0.95 eV is nearly the same for both cells as is the low barrier ~ 0.3 eV, the difference being in the area factor.

J-V-T MEASUREMENTS

The above analysis requires verification, so the barrier heights were also measured by barrier transport analysis using J-V data over a range of temperatures.

The usual treatment of thermal measurements [3-5], depends on the assumption of thermionic emission over the barrier. However, thermionic emission predicts a flat saturation, which is rarely seen in contact-dominated portion of the forward bias curves. This is usually dealt with by assuming a parallel resistance across the contact, although there should be some discussion about the origin and temperature dependence of such a parallel resistance.

Niemegeers et al. [6] used the drift/diffusion model for barrier transport [Sze] which allows a more gradual bias

dependence and fits the IEC data well, Fig. 5. This mechanism is more consistent with the diffusion velocities indicated by the charge densities and barrier heights in these cells. The cell model assumes a series combination of the main junction, fitted up to ~ 0.7 V with the usual

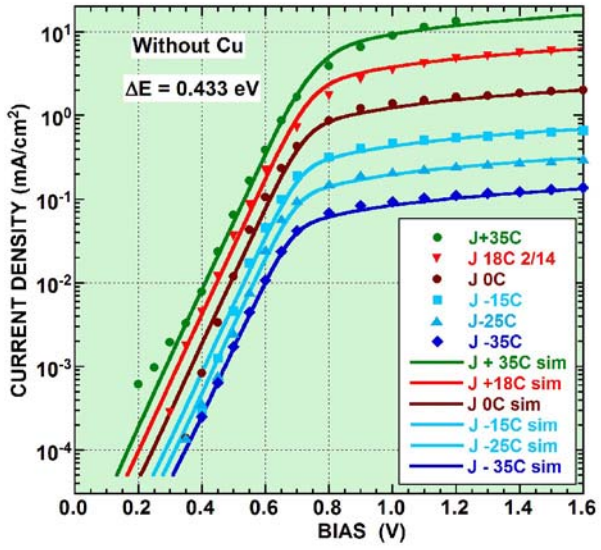

Fig. 5. Dark log J-V vs. T for IEC6. Points are experimental data, curves are drift-/diffusion model fit.

formulae, and a back contact with a J-V relation given by

$$J_{oc} = q\mu_h [2q(V_{dc} + V_c)N_a/\varepsilon_{ss}]^{1/2} N_{vb} \exp(-\Phi_c /kT)$$

$$J = J_{oc}[\exp(-qV_c/nkT) - 1] \qquad (3)$$

Once the proper values of μ_h, V_c and N_a were determined, all the model curves in Fig. 5 were generated by changing only T. There was good agreement between the J-V-T measurements and the IPE measurements for both of the IEC cells and the thin, unstressed cell.

Table 1. Drift/diffusion model properties

Hole mobility	μ_h	45 x (300/T) $^{3/2}$	cm^2/V-sec
Contact diffusion voltage	V_{dc}	$q\Phi_{bc}$ – kT ln (N_v/N_a) set at 0.05 V	V
Hole density	N_a	3e14	cm^{-3}
Permittivity	ε_{ss}	9.4 x 8.85 e-14	F/cm
Valence band density of states	N_{vb}	1.8e19 x (T/300) $^{3/2}$	cm^{-3}
Ideality factor	n	1	
Electric field in CdTe	E	$[q(V_{dc} + V_c)N_a/\varepsilon_{ss}]^{1/2}$ ~ 3e3	V/cm

where V_c is the voltage across the contact.

Barrier height measurements are summarized in Table 2.

Table 2. Barrier height comparison by method.

CELL	DRIFT/DIFF	THERMIONIC	IPE	AMPS
IEC6	0.387	0.344	0.37	
IEC3	0.433	0.388	0.43	
THIN unstressed	0.392	–	0.38	0.42
THIN stressed	~ 0.3	–	0.36	0.36
NREL <Opt		–		
NREL Opt	indeterminate	–	0.27	
NREL >Opt		–		

THIN CELLS

The thin cells both had ~ 1.8 μm CdTe layers. The unstressed cell TC-U had a normal J-V, while the stressed cell TC-S, chosen for its severe roll-over, had a ff ~ 0.3, Fig. 6 top. The IPE results were Φ_1 = 0.37 eV and $\Phi_{bc,eff}$ ~ 0.38 eV for TC-U and Φ_1 = 0.25 eV and $\Phi_{bc,eff}$ ~ 0.36 eV for TC-S. The IPE results show the contact to be a slightly different type than that for the IEC cells, with a higher second barrier at ~ 1.09 eV for TC-S.

The diffusion/drift transport measurement was a good fit for TC-U, giving Φ_{bc} = 0.39 eV, but was indeterminate for TC-S. The observation of a lower $\Phi_{bc,eff}$ and a smaller low barrier for the TC-S than the unstressed cell, despite its low ff, suggests that the J-V curve distortions are due to bulk transport effects, most likely in the CdTe, rather than due to the contact.

Simple AMPS simulations of the two thin samples tend to support this view. The thin cells were modeled giving the J-V plots and band diagrams in Fig. 6. The principle differences between the two AMPS models are the donor and acceptor densities.

Cell	N_d (cm^{-3})	N_a (cm^{-3})
Thin, unstressed, TC-U	2.5e15	3.5e15
Thin, stressed, TC-S	2.6e15	2.4e15

For TC-U the donor level is below the electron quasi-Fermi level over most of the CdTe, so the acceptors are not compensated. However, for TC-S, in the back of the CdTe the donor charge exceeds that of the acceptor charge giving the opposite band curvature, reducing the light-generated current $J_L(V)$ strongly for increasing forward bias, as observed for both the experimental data and AMPS simulation. It appears that the ff is reduced by low collection [$J_L(V)$] due to the saddle in the conduction band rather than by back contact resistance.

Taken together, these measurements and models suggest that the primary effect of the stressing for this device was not to change the contact barrier height but instead to reduce the net charge density $N_a - N_d$ in the bulk CdTe layer.

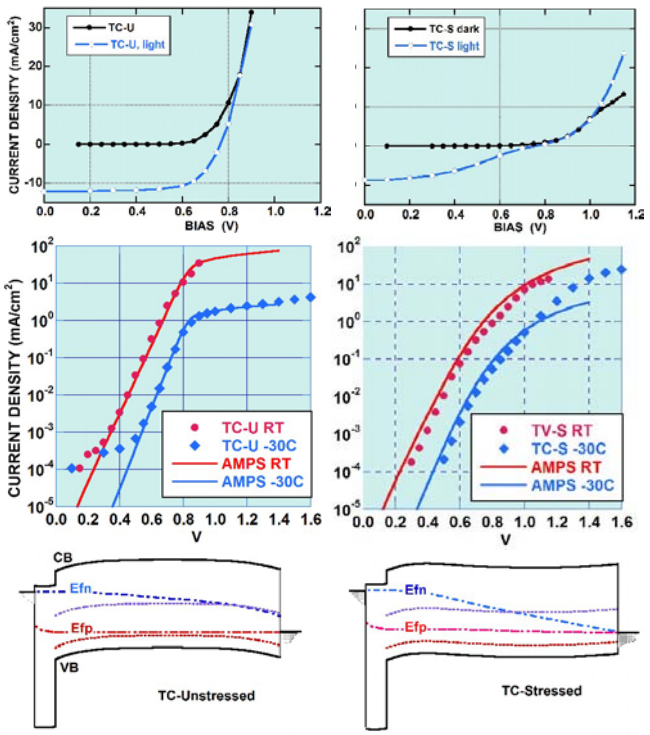

Fig. 6. Thin cell plots: left, unstressed; right, stressed. Top:light and dark linear J-V experimental data Middle: dark, log J-V at 18C and – 30C (points are experimental data, curves are AMPS simulation. Bottom: band diagrams at 0.7 V forward bias, dark, showing donor levels at CB – 0.75 eV and acceptor levels at VB + 0.2 eV. From AMPS simulation.

NREL CELLS

The NREL cells are electronically thick and have Cu-diffused ZnTe back contacts. NREL Opt3 with an optimum Cu diffusion has normal J-V characteristics with small crossover and no apparent roll-over at RT. On cooling the cross-over becomes very large, but the high forward bias

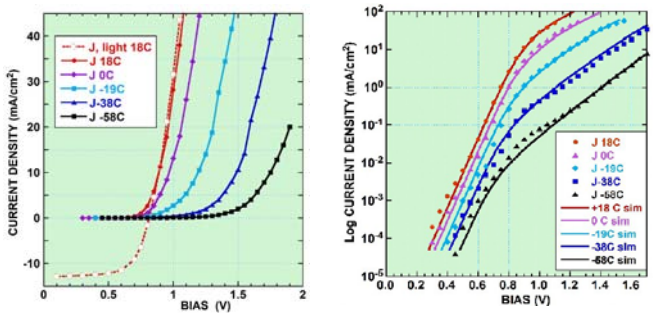

Fig. 7. Linear and log J-V for NREL Opt3. Points are experimental data. Log J curves are 2 diode model fit.

resistance remains relatively constant (Fig, 7) with no rollover, even at –58°C.

The dark log J-V curves are fit well with two diodes in series, both with the same polarity. The first has J_{o1} = $2x10^{-12}$ A/cm^2 and A_1 = 2.3, and the second has J_{o2} = $7x10^{-6}$ A/cm^2 and A_2 = 5 with an activation energy of ~ 0.5 eV. The effect of a reverse-biased back contact barrier, if present, appears to be negligible. The non-optimum Cu-diffusion cells both show extreme cross-over at RT.

The IPE results for NREL Opt3 (Fig. 8), show a low barrier intercept of 0.15 eV. The identification of this barrier

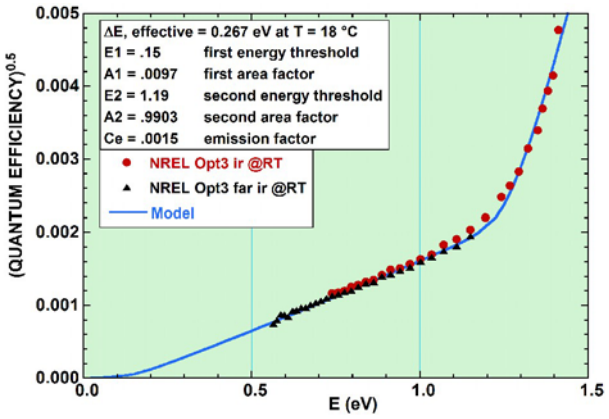

Fig. 8. Fowler plot for NREL Opt3 cell.

is unclear: it could be the valence band discontinuity ΔE_{vb} at the CdTe/ZnTe interface, measured by ARPES to be ~ 0.0 eV by Rioux [17], or it might be the ZnTe/metal barrier at the back of the cell. The low value is consistent with the lack of an apparent reverse-biased back barrier in the J-V curves.

These results suggest that the cross-over is due to bulk effects rather than a contact limitation

IPE AT REDUCED TEMPERATURES

The LIA signals at the longest wavelengths were small and noisy, requiring long data collection times. Cooling the cell was expected to increase sensitivity and accuracy. Cooling to –10°C did increase the signal by 20-fold, as modeled, but did not improve the signal-to-noise ratio. An unexpected result of cooling was an increase in the effective barrier height, e.g., from 0.37 eV at RT and 0°C, to 0.56 eV at – 25°C. This changed mainly the low barrier, increasing its height and decreasing its area. For the same cell, all the high energy log QE vs. E shapes are the same for all temperatures. This implies that the high barrier height is relatively independent of temperature.

CONCLUSIONS

The consistent shapes of the IPE Fowler plot curves for all the devices suggest that two barrier heights are present, one of which, 0.8 to 1.2 eV, is within the range of values commonly observed for single-crystal p-CdTe/metal contacts, and the other, 0.25 to 0.35 eV, is smaller than the cell limit value. Modeling the couples as two area-weighted barriers in parallel gives good agreement with the IPE data for most of the devices measured and allows calculation of effective thermionic barrier heights $\Phi_{bc,eff}$ for the barrier couples. These $\Phi_{bc,eff}$ are found to be in good agreement with barrier heights obtained from diffusion/drift transport modeling of J-V-T data. An alternative model involving tunneling could also explain the data, but IPE cannot differentiate between the two. For both IEC cells, the low IPE barriers are at a single height of 0.28 to 0.32 eV, with a small area factor (or tunneling probability) (~1-4%), while the

higher barrier is at ~ 0.95 eV. The higher $\Phi_{bc,eff}$ for IEC3 (without Cu, 0.44 eV) relative to IEC6 (with Cu, 0.37 eV) appears to be because of decreased area (or decreased tunneling probability) of the smaller barrier height component rather than a change in either high or low barrier heights.

The lower barrier heights (Φ_1) observed by IPE are consistent with the valence band offsets observed by Niles et al. [18] by XPS, ΔE_{vb} = 0.26 eV, for evaporated Te films on p-CdTe PX layers.

The existence of two parallel barriers offers an explanation of the apparent barrier height paradox, that SX CdTe values and most PX UPS Φ_{bc} values (except for that inferred by Niles [18]) are much larger than the solar cell limit. The small area (or low tunneling probability) would not be seen by UPS.

It is also consistent with observations of laterally inhomogeneous barriers (so-called patch barriers) discussed by Mönch [19] and Tung [20]. Parallel barriers are also suggested by the observations of Sutter [21] in PX CdS/CdTe/ZnTe cells, using charge injection spectroscopy with an STM. They found that the CdTe/ZnTe back contact current is highly non-uniform, involving large areas with roughly constant high contact resistance coexisting with small low resistance pathways, mostly at the grain boundaries. The scanning BEEM experiments of Fowell et al. [22] of Au/n-CdTe SX, also show very non-uniform barrier heights.

Possible causes of the lower barrier are mostly 3 dimensional effects, including intersections of the CdTe grain boundaries with the contact [21] and in-diffusion of Cu into the grain interfaces. This might either change the dipole locally to give areas of smaller Φ_{bc} or form tunneling regions. They might also include $Cu_{2-x}Te$ precipitates at the interface as suggested by Teeter [23].

The IPE method offers some special capabilities with respect to other methods. IPE is:

1. potentially able to separate contact effects from bulk transport effects and so is less ambiguous than thermal methods for electronically thin and n/i/p devices,
2. done on completed cells, in air at RT and above, or below RT in vacuum,
3. not affected by reasonable values of series or parallel resistance, either in the cell or at the contact,
4. done at bias voltages near the cell operating point, and
5. a relatively inexpensive extension to conventional QE measurement systems.

IPE is, of course, not without its complications:

1. Possible involvement of the competing electron barrier $\Phi_{bc,e} = E_g - \Phi_{bc,h}$ for thin n/i/p cells.
2. Possible influence of secondary photoconductivity.
3. The assumption of equal barrier collection coefficients may be questionable.
4. Interpretation of barrier height in terms of area vs. tunneling is not firm.
5. Small signal-to-noise ratio at low energies.

Potentially, with increased light flux, extended photon energy range, and better electronics, IPE could give barrier height values ± 0.01 eV. It is not yet an easy measurement, but when automated it could evolve into a rapid diagnostic to give more direct feedback for contact research. It is a good partner for thermal and UPS measurements, as well as BEEM, SKPS, and other STM techniques. IPE's best use is in context with other measurements.

ACKNOWLEDGEMENTS

I'd like to express my appreciation to Brian McCandless and Tim Gessert for cells used in these experiments and to Steve Hegedus, Al Enzenroth, and Jim Sites for helpful discussions.

REFERENCES

1. A. Klein, "*Advances in Solid State Analysis,*" 44, Springer (2004) p. 13.

2. B. Späth et al., *Thin Solid Films* 515, 6172 (2007).

3. G. Stollwerck and J.R. Sites, *Proc. 13th European PVSEC* (1995) 2020-2023.

4. B.E. McCandless, J. Phillips, and J. Titus, *Proc. 2nd WCPEC* (1998) 448-452.

5. S.H. Demtsu, J.R. Sites, *Thin Solid Films* **510,** 320–324 (2006).

6. A. Niemegeers and M. Burgelman, *J. Appl. Phys.*, **81**, 2881-2886(1997).

7. A.L. Fahrenbruch, *Mater. Res. Soc. Proc*. 1012, Y07-05 (2007).

8. S.M. Sze, "*Physics of Semiconductor Devices*," Wiley.

9. R.H. Fowler, *Phys. Rev*. 38, 45 (1931).

10. F. Urbach, *Phys. Rev*. 92, 1324 (1953)

11. D.T.F. Marple, *Phys. Rev*. 150, 728 (1966)

12. A. Fischer et al., *Appl. Phys. Lett.* 70, 3239 [1997]

13. R.H. Bube, "*Photoconductivity of Solids*," Wiley (1967) p. 79.

14. R.S. Crandall, *14th IEEE Photovoltaic Specialist's Conf.* (1980) p. 1221

15. S. Hegedus and J.M. Cebulka, *IEEE Photovoltaic Specialist's Conf.* (1988) p. 186.

16. T. Okumura and K.N. Tu, *J. Appl. Phys*. 54, 922 (1983).

17. D. Rioux, D.W. Niles, and H. Höchst, *J. Appl. Phys.* **73**, 8381 (1993).

18. D.W. Niles, X. Li, P. Sheldon, and H. Höchst, *J. Appl. Phys.* **77**, 4489 (1995).

19. W. Monch, "*Electronic Properties of Semiconductor Interfaces*," Springer-Verlag, Berlin (04) ch. 4.

20. R.T. Tung, *Mater. Sci. Reports* 35, 1-138 (2001).

21. P. Sutter et al., *Appl . Physics Lett.*; 84, 2100 (2004)

22. A. E. Fowell, R. H. Williams, B. E. Richardson, and T-H Shen, *Semicond. Sci. Technol*. 5, 346 (1990).

23. G. Teeter, *J. Appl. Phys*. 102, 034504 (2007)